AP7, a Partially Disordered Pseudo C-RING Protein, Is Capable of Forming Stabilized Aragonite in Vitro[†]

Fairland F. Amos and John Spencer Evans*

Laboratory for Chemical Physics, New York University, 345 East 24th Street, New York, New York 10010

Received November 21, 2008; Revised Manuscript Received December 22, 2008

ABSTRACT: AP7 is an extracellular aragonite-associated protein of the nacre layer of the mollusk *Haliotis rufescens* and possesses a 36-amino acid C-terminal domain that exhibits sequence homology to the C subclass of the RING domain intracellular protein family. We report here novel findings which implicate AP7 as a member of the intrinsically disordered protein class (IDP) and reveal new aspects of AP7 mineralization activity. AP7 is partially disordered but can undergo additional folding in the presence of TFE. AP7 binds Zn(II) ions in a non-tetracoordinate complex but does not require Zn(II) either for folding or for in vitro function. In addition to limiting calcite crystal growth, AP7 is also observed to induce aggregate formation within in vitro mineralization assays, and these aggregates are either amorphous (type A) or crystalline (type B) in appearance. The type A aggregate displays an irregular morphology and round, dark, electron dense deposits that do not give rise to a diffraction pattern. In contrast, the type B aggregates possess either organized parallel crystal clusters or highly dense hexagonal clusters that are confirmed by electron diffraction to be aragonite. This stabilization of aragonite is remarkable in that it occurred in the presence of AP7 alone and did not require typical aragonite stabilization agents such as Mg(II), other nacre proteins, or an organized organic matrix. The ability of a partially disordered C-RING protein to perform inorganic phase stabilization represents a new twist on both the RING domain and IDP stories, and this process of aggregate formation may provide an important clue with regard to the protein-mediated nacre formation process.

The formation of biominerals in Nature often requires the participation of specialized proteins that direct matrix assembly, nucleation, and crystal growth (*1, 2*). In many cases, the sequences of these specialized proteins are highly unique and often feature regions which do not correspond to the sequences of other known globular proteins (*3*−*7*). However, there have been observations of imperfect sequence homology between certain regions of biomineralization proteins and non-mineral-associated globular proteins (*4, 5, 7*). There is speculation that these globular-like domains have functions that are not directly related to nucleation or crystal interaction (*5, 8*). Some recent examples can be found in mollusk shell mineralization proteins, where regions homologous to acetylcholine-binding domains (*5*), glycine loops (*8*), and disulfide core domains (*8*) have been identified. An unusual example is AP7,[1] a 66-amino acid 7.5 kDa protein of the nacreous layer of the Pacific red abalone, *Haliotis rufescens* (*4, 9*), that possesses a C-terminal region that exhibits partial homology to an interesting subset of carboxy-terminal Cys-rich Zn binding motifs known as RING (really interesting new gene; C-RING subset) (*10*−*15*). Reported variants of the RING domain family occur in more than 400 proteins and bind either one or two Zn(II) ions per motif (*11*−*15*); in general, these domains are involved in mediating protein protein interactions within eukaryotic cells (*11*−*15*).

The similarities between the C-RING protein family and AP7 are intriguing for the following reasons. First, it is known that the AP7 protein copurifies as a noncovalent complex with another nacre-specific protein, AP24 (*4*), and from this we infer that protein−protein recognition may be another attribute of the AP7 protein. Second, analysis of the nacre layer has revealed that Zn(II) is present at detectable levels (0.72 ppm) within the mineral phase of one mollusk, although the presence of Zn(II) is not completely understood (*16*). Thus, a pseudo-Zn(II) motif within the AP7 sequence may have important implications for the nacre formation process. Recently, to secure additional information about RING domains, we reported on in vitro mineralization and biophysical studies of a synthetic peptide representing the C-RING—containing 36-amino acid C-terminal sequence of AP7 (AP7C) (*9, 10*). AP7C was found to exert no observable effect on Kevlar-nucleated in vitro calcium carbonate crystal growth (*9*). Unlike Zn(II) finger polypeptides (*17*−*19*), AP7C partially folds without the assistance of Zn(II) to form a global conformation consisting of three short helical segments that are interconnected by nonhelical regions (*10*). Further, we observed that the AP7C sequence binds Zn(II) in either 1:1 or 1:2 peptide−Zn(II) complexes but does not appear

[†] This work was supported by funding from the Department of Energy (DE-FG02-03ER46099).

* To whom correspondence should be addressed. Telephone: (212) 998-9605. Fax: (212) 995-4087. E-mail: jse1@nyu.edu.

[1] Abbreviations: AP7, aragonite protein 7; AP7C, 36-amino acid C-terminal domain of AP7; AP7N, 30-amino acid N-terminal domain of AP7; n16N, N-terminal fragment of aragonite associated oyster shell protein n16; RING, really interesting new gene; IDP, intrinsically disordered or unfolded protein; MALDI-TOF, matrix-assisted laser desorption ionization time-of-flight; PAM, (phenylacetamidomethyl) resin; tBOC, *tert*-butoxycarbonyl.

10.1021/bi802148r CCC: $40.75
Published on Web 01/21/2009

to utilize a tetracoordinate binding scheme that is typically found in Zn(II) finger polypeptides (*10*−*15*). Collectively, these initial findings suggested that the AP7C fragment exhibited atypical RING-like features and that this domain may participate in other features of the shell mineralization process, such as the formation of protein−protein complexes (*10*).

To follow up on these initial findings, we have now pursued direct investigations with AP7. Previous studies revealed that reduced apo-AP7 consists of random coil and α-helical structures and that the protein acts as a calcite "blocker" within Kevlar in vitro mineralization assays (*9*). Using the approaches devised in our recent AP7C studies (*10*), we have reinvestigated the structural and functional aspects of AP7 in more detail. In this report, we find that apo-AP7 is a partially disordered protein consisting of random coil and β-turn, β-sheet, and helical conformations. This protein undergoes structural stabilization in the presence of external agents such as TFE, and in this regard, AP7 appears to be similar to other intrinsically disordered proteins (IDPs) (*20, 21*). We also confirm that the Zn(II) binding properties of AP7 are identical to those of the AP7C fragment (*10*); i.e., both AP7C and AP7 bind Zn(II) using a non-tetracoordinate scheme, and Zn(II) does not induce protein folding in either polypeptide. Perhaps the most important finding is that AP7 not only modulates the nucleation and morphology of calcite in vitro, but also simultaneously forms amorphous-like and aragonite-containing aggregates in solution without the need for other agents.

MATERIALS AND METHODS

Solid-Phase Synthesis, Purification, and Sample Preparation. The synthesis and purification of free α-carboxyl, free Cys-SH AP7 was conducted at the William Keck Biotechnology Peptide Synthesis Facility (Yale University, New Haven, CT) using Asn-trityl-PAM (phenylacetamidomethyl) resin, a customized Applied Biosystems 432A peptide synthesizer, and standard chemistry with in situ neutralization and subsequent protein purification under reducing conditions (*17*−*19*) as described previously (*9*). The lyophilized protein was subsequently dissolved in H_2/N_2-flushed deionized distilled water (final concentration of 500 μM), and the final pH was adjusted to 7.0 using NaOH. In essence, the protein acts as its own buffer under these conditions and remains soluble without evidence of aggregation. Aliquots were then stored at −20 °C in airtight sealed vials that were preflushed with high-purity N_2 gas. To ensure continued reducing conditions for AP7 Cys residues, all solutions utilized in the experiments described below were degassed and purged with high-purity N_2/H_2 gas for at least 15 min immediately prior to each experiment (*9, 10, 17*−*19*). Note that the reduced apo-AP7 was found to exhibit excellent solubility in the 4−500 μM range when stock solutions were diluted into neutral-pH, low-ionic strength aqueous buffers.

Metal Ion Binding Studies. AP7 metal ion binding studies was performed using a matrix-assisted laser desorption ionization time-of-flight (MALDI-TOF) Bruker OmniFlex MS spectrometer in the negative ion mode. The instrument contains a pulsed ultraviolet laser with a power of 200 mJ at 337 nm. The AP7 stock solution was diluted to 50 μM in a 1:9 (v:v) acetonitrile/20 mM ammonium acetate buffer (J. T. Baker Chemical Co.) at pH 7.4. AP7/metal ion mixtures were then created using metal ion stock solutions of $CaCl_2$, $ZnCl_2$, $LaCl_3$, and $EuCl_3$ (99.99%, Sigma-Aldrich). The final protein:metal ion ratio was 1:10. The matrix solution was ATT [6-aza-2-thiothymine, 99%, Sigma-Aldrich, dissolved in a 1:9 acetonitrile/20 mM ammonium acetate buffer (pH 7.4) to a final stock concentration of 10 mg/mL]. We created samples by premixing the AP7/metal ion mixture with the matrix solution in a ratio of 1:2, then applying this mixture directly to the MALDI target, and drying the aliquot at room temperature with a gentle stream of filtered compressed air. No additional washing steps were performed.

UV−*Vis Spectroscopy.* We utilized Co(II) as an analogue of Zn(II) to probe metal ion binding (*17*−*19*) of AP7, using the protocols published earlier for AP7C (*10*). AP7 samples [20 μM in 100 μM Tris-HCl (pH 7.4)] were created and titrated using stoichiometric amounts of a 1 M $CoCl_2$ stock solution (99.99% pure, Sigma-Aldrich, in deionized distilled water) to the apoprotein; final AP7:Co (II) stoichiometries of 1:1 to 1:300 were utilized. Ultraviolet and visible light spectra of Co(II)−AP7 complexes were recorded at 20 °C on an Agilent 8453 spectrophotometer. Spectra were obtained using 1 cm path length quartz cells (Sarna, Inc.), an integration time of 0.5 s, and an interval of 1 nm.

Circular Dichroism Spectroscopy. CD spectra of apo-AP7 and AP7 in the presence of Zn(II) and 2,2,2-trifluoroethanol (TFE) were recorded at 20 °C using an AVIV stopped-flow 202SF CD spectropolarimeter, using a total of seven scans per sample and a scan rate of 0.5 nm/s. For all studies, protein samples [10 μM in 100 μM Tris-HCl (pH 7.5)] were scanned from 185 to 260 nm. The CD spectrometer was previously calibrated with *d*-10-camphorsulfonic acid. For metal ion binding studies, microliter additions of a $ZnCl_2$ stock solution (99.9% pure, Sigma-Aldrich) were added to the diluted stock solution to create a range of AP7:metal ion stoichiometries (2:1, 1:1, and 1:10 AP7:metal ion ratios). For folding propensity studies, an AP7 sample was titrated with the solvent 2,2,2-trifluoroethanol (99.8% pure, Acros America) at varying volume percentages. Spectra were recorded with appropriate background buffer subtraction performed [where applicable TFE, Zn(II), and Tris-HCl]. The averaged spectra were smoothened using the Savitzky−Golay algorithm. Ellipticity is reported as mean residue ellipticity, θ_M (degrees square centimeter per decimole). Secondary structure estimation of AP7 was performed using a constrained least-squares fit of the AP7 CD spectra with a five-component model (α-helix, β-sheet, β-turn types I and II, random coil, and aromatic, disulfide contributions) utilized in the CD analysis software LINCOMB (*22*). The resulting fit was performed using IGOR Pro 6.0 and is reported as the fractional weight plus or minus the standard deviation of the five reference components.

In Vitro Mineralization Assays. We employed a polyimide (Kevlar) assay (*9, 23, 24*) for the nucleation of calcium carbonate crystals in the presence of AP7, using untreated polystyrene six-well tissue culture plates (3 mL assay volume per well). Total AP7 assay concentrations were 5×10^{-6}, 1×10^{-5}, 5×10^{-5}, and 1×10^{-4} M. Negative control conditions consisted of no added protein. Assay conditions and sample preparation for SEM imaging were as described in our previous studies (*9, 23, 24*).

In addition to the Kevlar fiber assay, we also ran parallel assays where no Kevlar fibers were introduced. These assays

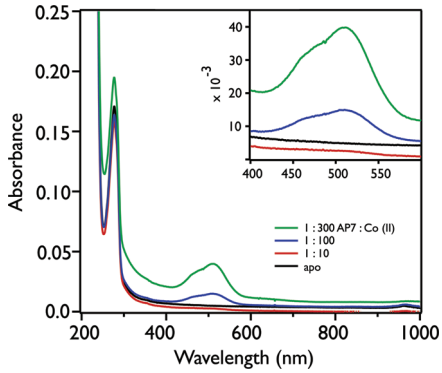

FIGURE 1: Absorption spectra of $CoCl_2$ in the presence and absence of stoichiometric amounts of the AP7 protein with 100 μM Tris-HCl (pH 7.4). Inset spectra show enlargement of the 400−600 nm wavelength region.

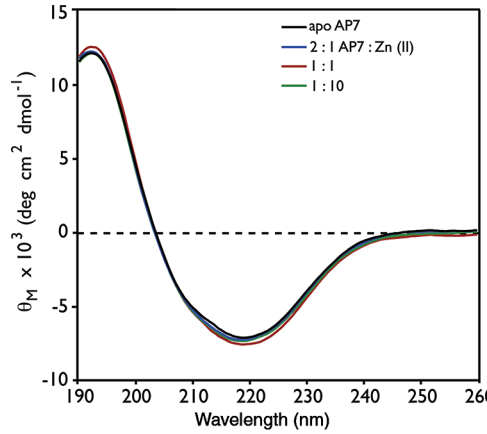

FIGURE 2: CD spectra of 10 μM AP7 in 100 μM Tris-HCl (pH 7.4) in the apo form and in the presence of stoichiometric amounts of $ZnCl_2$.

were utilized for analysis of the formation of mineralization clusters in solution. For TEM studies, an aliquot (~10 μL) of the assay supernatant was removed and carefully spotted on a copper TEM grid (coated with a Formvar layer that is stabilized by carbon; Ted Pella, Inc.). This spot was gently washed with ethanol and deionized distilled water. This spotting and washing procedure was repeated again using a fresh aliquot each time such that enough insoluble assay material would be deposited on the grids for subsequent visualization. Once sufficient aliquot transfers to the grids had been completed, the grids were allowed to air-dry. TEM imaging and electron diffraction measurements were performed on grids using a Philips CM12 transmission electron microscope at 120 kV. Cropping of TEM and SEM images and adjustment of brightness and darkness and contrast levels were performed using Adobe Photoshop.

RESULTS

AP7 Is a Metal Ion Binding Protein. Using MALDI-TOF and the metal ion-induced mass shift method (*25, 26*), we confirmed that AP7 binds Ca(II) (1:1 adduct), Eu(III) (1:1 adduct), and La(III) (1:1 and 2:1 adducts) (Table S1 and Figures S1−S3 of the Supporting Information). These data confirm that one or more Ca(II) binding sites are present within AP7. In the presence of Zn(II), we were able to identify 1:1 and 1:2 AP7−Zn(II) adducts (Figure S1 and Table S1 of the Supporting Information). These results are comparable with our earlier studies with AP7C, where one and two Zn(II) ions were observed to bind to this C-RING domain fragment (*10*). Subsequent UV−vis spectrophotometric characterization of Co(II) binding reveals that, like the AP7C fragment (*10*), the parent AP7 protein does not exhibit the coordination characteristics of Zn(II) finger polypeptides (Figure 1) (*17−19*). Typically, aqueous $CoCl_2$ possesses two bands in the visible region at 460 and 510 nm whose intensities are concentration-dependent (Figure 1) (*10, 17−19*). In the presence of Zn(II) finger polypeptides, the binding of Co(II) ion produces the characteristic strong d−d transitions seen between 550 and 725 nm in tetrahedrally coordinated complexes of this metal ion (*10, 17−19*). However, the stoichiometric addition of Co(II) to reduced AP7 does not reveal this d−d transition. Instead, we observe two peaks. The first is at 277 nm, which was previously reported as an indication of a possible ligand metal charge transfer (LMCT) coordination of Co(II) with AP7C (*10*). However, the reader should note that the LMCT band for typical Zn(II) finger sequences in the presence of Zn(II) has been reported to be much broader and exhibits a shoulder region at 310−350 nm (*17−19*), which is not evident in our AP7 UV−vis spectra (Figure 1). The other peak is observed at 510 nm and is assigned to the "unbound" hydrated $CoCl_2$ (*10, 17−19*). Hence, the UV−vis experiments confirm that AP7 does not form a tetracoordinate complex with Co(II) like other Zn(II) binding proteins (*17−19*). Combining this result with our MALDI-TOF data leads us to the conclusion that the ligand coordination number for AP7−Zn(II) interactions must be either mono-, bi-, or tridendate.

AP7 Is a Partially Disordered Protein. Previous structural studies of the N- and C-terminal domains of AP7 demonstrated that the mineral-modifying 30-amino acid N-terminal region existed as an unfolded species in solution (*26a, 26b*), but the 36-amino acid C-terminal pseudo C-RING domain possessed a partially disordered α-helical conformation in the presence and absence of Zn(II) (*10*). Apo-AP7 in Tris-HCl buffer was found to share the same structural features of its two subdomains, namely, the presence of both random coil-like structure and α-helix (*9*). This is shown in Figure 2, where we observe three ellipticity bands for reduced apo-AP7: a (+) band centered at 192 nm (random coil), a weak, broad (−) band at 208 nm ($\pi-\pi^*$ transition), and a (−) band at 222 nm (n−π^* transition) (α-helix) (Figure 2; secondary structure classifications for apo-AP7 are given in Table 1). Interestingly, with the addition of Zn(II), the n−π^* and $\pi-\pi^*$ transitions for AP7 persist and do not exhibit significant changes in ellipticity intensity or wavelength (Figure 2). These findings are similar to what we obtained for AP7C (*10*), and we conclude that the addition of Zn(II) does not appreciably change the global structure of AP7.

The presence of structural disorder is essential for the function of a number of protein sequences (*9, 10, 21, 23−28*), where local folding or reordering occurs during molecular recognition of other molecular entities (*21*). In previous studies with AP7N, we determined that this mineral-modifying sequence exists in an intrinsically disordered state but can be further stabilized by the structure-stabilizing solvent, 2,2,2-trifluoroethanol (TFE), to fold into an α-helical conformation (*26*). The presence of AP7N folding propensity was also noted in recent X-ray studies which demonstrate that, relative to the solution state, the AP7N sequence

Table 1: Secondary Structure Estimates for Apo-AP7 Using the LINCOMB Reference Set[a]

α-helix		β-structure[b]		random coil	
0% (v/v) TFE	75% (v/v) TFE	0% (v/v) TFE	75% (v/v) TFE	0% (v/v) TFE	75% (v/v) TFE
0.121 ± 0.011	0.252± 0.006	0.341 ± 0.086	0.286± 0.045	0.268 ± 0.059	0.283± 0.031

[a] Percentages represent fractional weights of each secondary structure type. [b] Includes β-turns and parallel and antiparallel β-sheets.

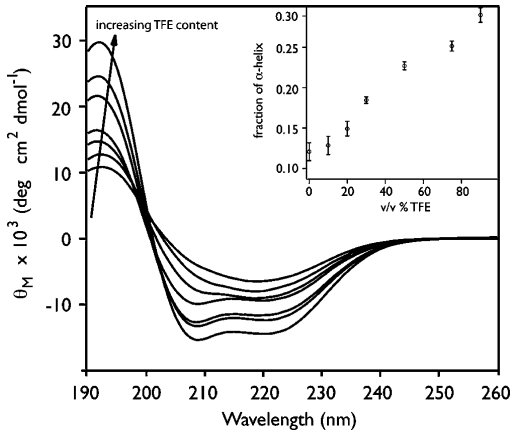

FIGURE 3: CD spectra of 10 μM AP7 in the presence of varying percentages of TFE. The inset shows the percentage of α-helical structure formed as a function of TFE content. Percentages of secondary structure classifications for 0% (v/v) and 75% (v/v) TFE were determined from the LINCOMB data set (*22*) and are given in Table 1.

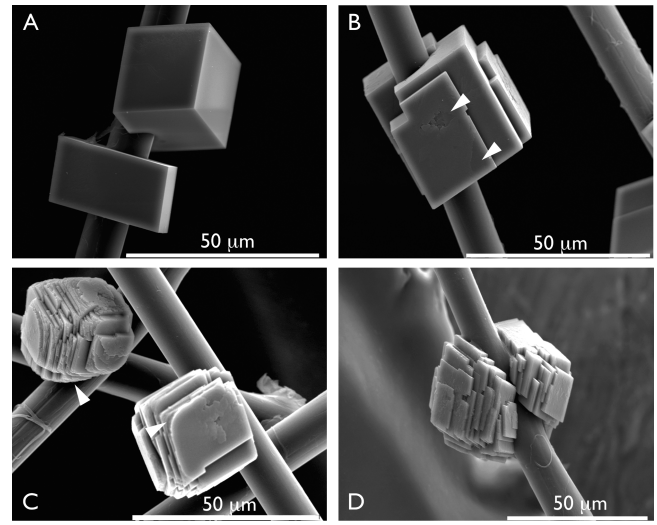

FIGURE 4: Scanning electron micrographs of the rhombohedral calcite crystals nucleated on Kevlar threads: (A) negative control and (B−D) 5, 10, and 100 μM AP7, respectively. In panel B, arrows point to the surface coarsening and rounding of calcite step edges observed in the presence of AP7. Panel C shows the seldom observed rounded step edges due to the interaction of AP7 on the (104) planes.

undergoes side chain reordering when adsorbed onto calcite (*27*). To determine if the AP7 protein is likewise transformable, we utilized the structure-stabilizing solvent, TFE (*29*), to probe the folding propensities of reduced, annealed apo-AP7 (Figure 3). As noted in Figure 3, the resolution and intensities of the (−) 208 nm ($\pi-\pi^*$) and 222 nm ($n-\pi^*$) transitions, which are signature bands for α-helical conformation, increase as a function of TFE content. Using CD database reference spectra (*22*), we estimated the percentage of helical, β-structure (i.e., turn and sheet content), and random coil structures in apo-AP7 at 0 and 75% (v/v) TFE (Table 1). We note that relative to the 0% TFE sample, the helical content in the 75% TFE sample nearly doubles, with the content of β-structures and random coil conformation remaining constant in both samples within statistical limits. This phenomenon is also mirrored in the inset plot of Figure 3, where the α-helical content of AP7 is observed to proportionally increase as a function of TFE content. Thus, our current data now reveal that under conditions of external stabilization, additional folding occurs within AP7 (Figure 3 and Table 1). The presence of additional folding reflects a disorder-to-order transition brought about by external agents (*26c, 29, 30*), and we note that such transitions have been noted in a number of IDP proteins (*20, 21*).

In Vitro Mineralization Activity of AP7, Revisited. In earlier studies, AP7 and its N-terminal fragment, AP7N, exhibited "blocking" activity of calcite crystal growth upon Kevlar threads (*9*). These observations were obtained for an AP7 concentration range of 5−50 μM. Subsequent to our initial findings for AP7 (*9*), we found that a Cys-containing nacre-specific polypeptide was capable of forming mineralized biofilms at peptide concentrations of 100 μM (*23*). Given that AP7 also contains Cys residues, it occurred to us that AP7 might self-assemble at higher concentrations (>50 μM), leading to the formation of protein-based biofilms or aggregates. Thus, we decided to reinvestigate AP7 mineralization behavior over a broader range of different concentrations (5, 10, and 100 μM) within in vitro assays (Figure 4) (*9, 23, 24*). At 5 μM AP7 (Figure 4B), we observe minor interruption in the growth of the Kevlar-nucleated rhombohedral calcite crystals, which is not observed in the control $CaCO_3$ assays (Figure 4A). As indicated by the arrows in Figure 4B, the (104) surfaces of the calcite crystals appear coarse and feature rounded step regions due to the blocking interaction of AP7, and similar results were noted in our earlier AP7 mineralization studies (*9*). At 10 μM AP7, we note that the rounding of calcite surface step regions is increasing and that this phenomenon has now progressed to the corner and edge regions of these crystals (Figure 4C). Finally, at 100 μM AP7, we see that the AP7 protein is now promoting the formation of polycrystalline aggregates that feature multiple terraces with rounded step regions (Figure 4D). Hence, there is an AP7 concentration-dependent effect on calcite crystal growth and morphology.

Interestingly, in assays containing 100 μM AP7, we noted the simultaneous appearance of a gel-like substance or coating on a small fraction of the calcite crystals and Kevlar threads in the assay (Figure 5A) which was not observed in the negative control assays (Figure 4A). This coating of Kevlar-induced crystals appeared to be random and was not widespread. This led us to believe that these coatings formed in solution and were randomly deposited on the Kevlar-nucleated crystals as the supernatant was withdrawn at the end of the assay period. To verify this, we ran parallel mineralization assays under identical conditions but omitted the Kevlar threads (Figures 5 and 6) and analyzed the assay

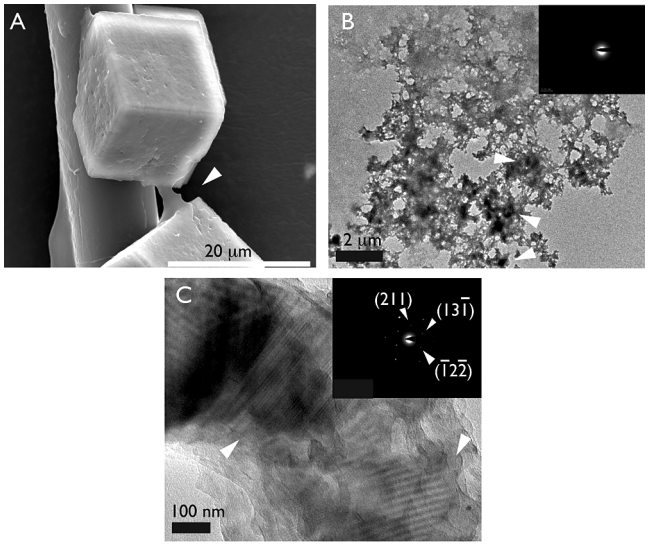

FIGURE 5: AP7-induced aggregate formation. (A) Scanning electron micrograph of the gel-like coating observed on Kevlar-nucleated calcite crystals in the presence of 100 μM AP7. (B and C) Transmission electron micrographs of (B) disordered, amorphous-appearing and (C) ordered, crystalline aggregates formed in the assay solution in the presence of 100 μM AP7. The presence of electron-dense, dark deposits is noted in panel B (white arrows). Insets show the corresponding electron diffraction patterns obtained from these samples (see Table 2). In panel C, the aragonite diffraction pattern was taken along the [4 $\bar{3}$ 5] direction of the sample.

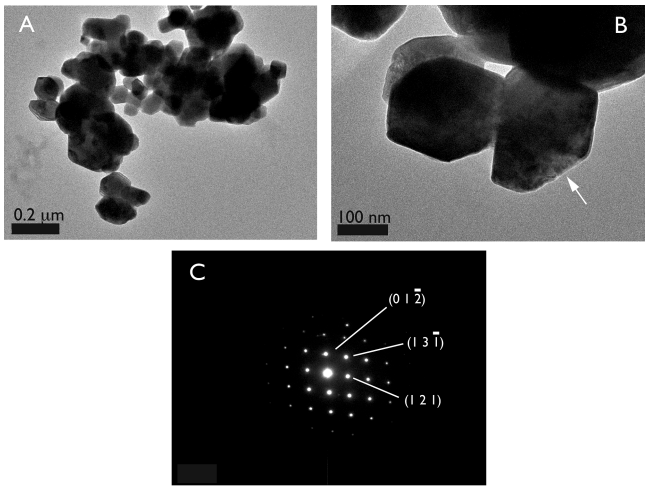

FIGURE 6: (A) Transmission electron micrographs of an AP7-induced aggregate containing an assembly of mineralized tablets. These aggregates are formed in the presence of 100 μM AP7. (B) A higher magnification of a mineralized tablet. In both panels A and B, note the hexagonal shape of the tablets. In panel B, the arrow indicates where the electron diffraction pattern in panel C was recorded. The observed Miller indices correspond closely with that of aragonite (see Table 2), taken along the [$\bar{5}$ 2 1] direction.

supernatant for the presence of suspended aggregates (Figure 5B,C). TEM imaging confirmed the presence of two classes of aggregates in the AP7 supernatants. The first class appeared to be amorphous (Figure 5B), and the second class appeared to be crystalline (Figure 5C). The amorphous aggregates have an irregular border, and there is evidence of dark, electron-dense regions which suggests the presence of mineralization (note the arrows pointing to dark regions in Figure 5B). However, none of these regions in the amorphous films generated a diffraction pattern (for example,

Table 2: Experimental and Theoretical *d* Spacing and θ Angle Values for the Diffraction Patterns in Figures 5 and 6

crystallographic plane/angle	theoretical value	experimental value
Diffraction Patterns in Figure 5		
$d_{(2\,1\,\bar{1})}$	0.219 nm	0.218 nm
$d_{(1\,3\,\bar{1})}$	0.217 nm	0.217 nm
$d_{(\bar{1}\,2\,\bar{2})}$	0.211 nm	0.212 nm
$\theta_{(2\,1\,\bar{1}),(1\,3\,\bar{1})}$	62.2°	61°
$\theta_{(1\,3\,\bar{1}),(\bar{1}\,2\,\bar{2})}$	58.4°	59°
$\theta_{(2\,1\,\bar{1}),(\bar{1}\,2\,\bar{2})}$	120.6°	120°
Diffraction Patterns in Figure 6		
$d_{(0\,1\,\bar{2})}$	0.270 nm	0.270 nm
$d_{(1\,3\,\bar{1})}$	0.217 nm	0.221 nm
$d_{(1\,2\,1)}$	0.273 nm	0.272 nm
$\theta_{(0\,1\,\bar{2}),(1\,3\,\bar{1})}$	50.8°	51°
$\theta_{(1\,3\,\bar{1}),(1\,2\,1)}$	51.6°	52°
$\theta_{(0\,1\,\bar{2}),(1\,2\,1)}$	102.4°	103°

see Figure 5C), and this suggests that if a mineral phase is present in these films, then it may be amorphous calcium carbonate (ACC). The second class of aggregate appeared more organized and dense, and we noted two different types. One type features very thin, nonfaceted crystalline deposits, presumably in their early stage of film growth where lattice fringes are visible (Figure 5C). Careful diffraction pattern matching (*d* spacing and θ angle) of these crystalline samples against calcite, aragonite, and vaterite reveals a good match with the aragonite polymorph (Table 2), with minor deviations. The other type appears as rounded clusters of hexagonal platelets that are denser and possibly represent a later stage of aggregate development (Figure 6A,B). Here, the lattice fringes are no longer observed. These aggregates also give rise to diffraction patterns that correspond closely to aragonite (Figure 6C and Table 2). We believe that the lattice distortions in both crystalline types arise from protein-induced distortions in the mineral phase. This conclusion is supported by similar evidence obtained for calcite crystals containing sea urchin intracrystalline proteins (*31*), and for AP7N-adsorbed calcium carbonates which exhibit chemical distortions in the crystal surface (*27*).

Collectively, we interpret our TEM data as follows. Two classes of aggregates, type A and type B, form in the AP7 mineralization assays. The first class, type A, appears disordered and may contain amorphous calcium carbonate (ACC) as evidenced by the presence of diffuse electron diffraction patterns (Figure 5B). Given the small size of the aggregate and the limited quantities available, we were unable to pursue complementary methods of analysis, such as FT-IR or Raman spectroscopy, to confirm the presence of ACC in these samples. A second class of aggregate, type B, was also identified (Figures 5C and 6), and these complexes are denser, are more organized in appearance, and contain aragonite (Figures 5C and Figure 6 and Table 2) but exhibit different morphologies and mineral crystal organization. Hence, the AP7 nacre protein appears to be multifunctional and not only can limit calcite crystal growth as we originally observed (Figure 4) (*9*) but also can promote amorphous and crystalline aggregate formation, with evidence of aragonite stabilization in the latter case (Figures 5 and 6). The ability of a single protein that can stabilize aragonite in vitro in solution without additional agents is noteworthy, since previous reports held that protein-stabilized

aragonite required either Mg(II) (*3*) or multiple mollusk shell proteins (*32*) to accomplish this task.

DISCUSSION

In previous work, we established that the 36-amino acid C-terminal domain of AP7 represents a pseudo C-RING partially helical sequence that binds Zn(II) ions but not in a tetracoordinate complex that is typical of Zn(II) finger polypeptide sequences (*10, 18*−*20*). We also established that the 30-amino acid N-terminal domain of AP7 exists in a disordered state (*26*) and is capable of modulating calcite crystal growth in vitro with evidence of kinetic control over this process (*33*). Now, in the work presented here, we take these findings a step further and confirm that the parent protein, AP7, exhibits molecular traits that represent a composite of both N- and C-terminal domain sequence traits (Figures 1−5). The AP7 protein is partially disordered yet functional and consists of random coil structure as well as helical and β-structures (Table 1). This protein is conformationally transformable and undergoes structural reordering in the presence of TFE (Figure 3) but not in response to Zn(II) (Figure 2). As noted elsewhere, an important feature of the IDP protein class is the ability of certain disordered proteins to promote assembly formation (*21*), features that we now associate with AP7 (Figures 5 and 6) and with other IDP biomineralization proteins such as amelogenin (*34*) and starmaker (*35*). On the basis of these collective findings, we tentatively assign AP7 as an IDP protein and intend to pursue additional structural studies of this protein at a later date.

The most interesting finding is that AP7 can promote amorphous (type A) and crystalline (type B) aggregate formation in vitro (Figures 5 and 6), with evidence of aragonite stabilization within the type B aggregates (Figure 5C). The aragonite phase within the type B aggregate exhibits minor lattice distortions (Table 2), and we attribute these distortions to the presence of the AP7 proteins, although we do not know if these distortions are due to either intracrystalline localization of AP7 or AP7-induced disruption of the Ca(II)−CO_3^{2-} bonding at the crystal surfaces (*27*). Aragonite stabilization was achieved by AP7 alone and did not require the presence of Mg(II), Zn(II), or an insoluble organic matrix. Aggregate formation was not originally observed in our earlier AP7 studies (*4, 9*), and we attribute this to the use of higher AP7 protein concentrations (i.e., 100 μM) in the assays presented here. Unfortunately, little is known about the inorganic−organic composition of these aggregates or the actual chemical environment that creates conditions for phase stabilization within the aggregates, and further studies will be required to address these issues.

The ability of a partially disordered, pseudo C-RING extracellular matrix protein, AP7, to form mineral aggregates and promote phase stabilization represents a new twist on both the RING and IDP sagas. Since the pseudo C-RING sequence of AP7 does not play a direct role in in vitro mineralization (*9*), we speculate that this domain is modulating some portion of the AP7-mediated aggregation process. This hypothesis is supported by the general involvement of RING domains in intracellular recognition and assembly of proteins (*11*−*15*). What is intriguing about the AP7-mediated aggregate formation is that RING domains typically require Zn(II) to promote assembly (*15*),

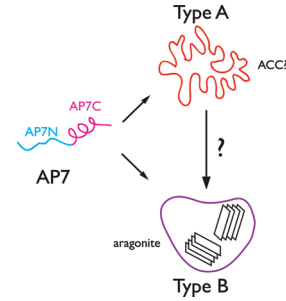

FIGURE 7: Proposed mechanism for AP7-mediated aggregate formation in vitro. AP7 somehow promotes the formation of two kinds of aggregates: one with an amorphous, irregular morphology with no evidence of a crystalline mineral phase (type A) and the other with a more ordered, dense appearance that exhibits aragonite stabilization (type B). In either type, we believe that the stabilization of biominerals within the aggregate results from chemical environments created by AP7 side chains. The question mark indicates that we do not know if these pathways are sampled. ACC? indicates that the type A aggregate may contain amorphous calcium carbonate (ACC), but the physical confirmation of this is lacking at present.

but here aggregates are forming in the absence of Zn(II) (Figures 5 and 6). The reason why Zn(II) may be unnecessary for the AP7-mediated aggregation process is probably due to the presence of a partial fold within the C-terminal domain of AP7 (*10*) which somehow conveys in vitro functionality to AP7 without a Zn(II) requirement. Note that these features diverge from what we typically associate with the intracellular RING protein family (*11*−*15*). However, given that Zn(II) is detected within invertebrate shell matrices in trace amounts (*16*), we cannot discount the possibility that Zn(II) has some specified effect on the in vivo function of AP7.

As to how AP7 promotes aggregation and aragonite phase stabilization in vitro, we propose a preliminary mechanism for this process (Figure 7). It is clear that partially disordered AP7 somehow creates conditions in solution where two types of aggregates are created (Figure 7). We speculate that the C-RING domain of AP7 somehow directs this process, and as pointed out for another aggregate-promoting nacre sequence, n16N (*26c*), free Cys thiol groups within the pseudo C-RING domain of AP7 could play an important role in the aggregation process. As to how phase stabilization occurs, we believe that the partially disordered, unstable conformation of AP7 somehow creates a suitable molecular environment of protein side chain groups that are conducive to mineral formation and aragonite stabilization (Figure 7). Given that the N-terminal 30-amino acid domain of AP7 has been shown to modulate mineral formation, we speculate that this sequence region of AP7 may be the major participant in the phase stabilization process. With regard to this model, three major questions remain unanswered. First, does aggregate formation arise as a result of AP7 self-association? This is an intriguing concept, for a self-assembled protein complex could generate an enclosed protein side chain microenvironment for phase stabilization of either ACC or aragonite. In fact, a similar process has already been identified in a disordered artificial inorganic nucleation protein, p288 (*30*), where the formation of protein supramolecular complexes created conditions where diffusion-limited nucleation of inorganic

crystals could occur. Second, what is the temporal relationship between type A and type B aggregates: does the amorphous type A aggregate form prior to the appearance of type B, or are they simultaneously formed? If the type A aggregate is a precursor to type B, then perhaps the appearance of type B is regulated by AP7 in some fashion. Finally, and most importantly, does AP7 promote the formation of mineralized aggregates and phase stabilization within the nacre layer of the mollusk shell, and if so, is the participation of other nacre proteins required? Future studies will resolve these issues.

ACKNOWLEDGMENT

This work represents contribution 51 from the Laboratory for Chemical Physics.

SUPPORTING INFORMATION AVAILABLE

Negative mode MALDI-TOF of apo-AP7 and AP7 in the presence of a 10-fold molar excess of $CaCl_2$, $ZnCl_2$, $LaCl_3$, or $EuCl_3$ at pH 7.4. This material is available free of charge via the Internet at http://pubs.acs.org.

REFERENCES

1. Mann, S., Webb, J., and Williams, R. J. P., Eds. (1989) *Biomineralization: Chemical and Biochemical Perspectives*, VCH, Weinheim, Germany.
2. Lowenstam, H. A., and Weiner, S. (1989) *On Biomineralization*, Oxford University Press, New York.
3. Samata, T., Hayashi, N., Kono, M., Hasegawa, K., Horita, C., and Akera, S. (1999) A new matrix protein family related to the nacreous layer formation of *Pinctada fucata*. *FEBS Lett. 462*, 225–232.
4. Michenfelder, M., Fu, G., Lawrence, C., Weaver, J. C., Wustman, B. A., Taranto, L., and Evans, J. S. (2003) Characterization of two molluscan crystal-modulating biomineralization proteins and identification of putative mineral binding domains. *Biopolymers 70*, 522–533 (errata in Vol. 73, p 522).
5. Ma, Z., Huang, J., Sun, J., Wang, G., Li, C., Xi, L., and Zhang, R. (2007) A novel extrapallial fluid protein controls the morphology of nacre lamellae in the pearl oyster, *Pinctada fucata*. *J. Biol. Chem. 282*, 23253–23260.
6. Fu, G., Qiu, S. R., Orme, C. A., Morse, D. E., and DeYoreo, J. J. (2007) Acceleration of calcite kinetics by nacre proteins. *Adv. Mater. 17*, 2678–2683.
7. Mann, K., Siedler, F., Treccani, L., Heinemann, F., and Fritz, M. (2007) Perlinhibin, a cysteine, histidine, and arginine-rich mini-protein from abalone (*Haliotis laevigata*) nacre, inhibits in vitro calcium carbonate crystallization. *Biophys. J. 93*, 1246.
8. Shen, X., Belcher, A. M., Hansma, P. K., Stucky, G. D., and Morse, D. E. (1997) Molecular cloning and characterization of Lustrin A, a matrix protein from shell and pearl nacre of *Haliotis rufescens*. *J. Biol. Chem. 272*, 32472–32481.
9. Kim, I. W., Collino, S., Morse, D. E., and Evans, J. S. (2006) A crystal modulating protein from molluscan nacre that limits the growth of calcite in vitro. *Cryst. Growth Des. 6*, 1078–1082.
10. Collino, S., Kim, I. W., and Evans, J. S. (2008) Identification and structural characterization of an unusual RING-like sequence within an extracellular biomineralization protein, AP7. *Biochemistry 47*, 3745–3755.
11. (a) van Baren, M. J., van der Linde, H. C., Breedveld, G. J., Barrends, W. M., Rizzu, P., de Graaf, E., Oostra, B. A., and Heutink, P. (2002) A double RING-H2 domain in RNF32, a gene expressed during sperm formation. *Biochem. Biophys. Res. Commun. 292*, 58–86. (b) Braun, M. A., Costa, P. J., Crisucci, E. M., and Arndt, K. M. (2007) Identification of Rkr1, a nuclear RING domain protein with functional connections to chromatin modification in *Saccharomyces cerevisiae*. *Mol. Cell. Biol. 27*, 2800–2811.
12. (a) Saurin, A. J., Borden, K. L. B., Boddy, M. N., and Freemont, P. S. (1996) Does this have a familiar RING? *Trends Biochem. Sci. 21*, 208–215. (b) Freemont, P. S. (2000) Ubiquitination: RING for destruction? *Curr. Biol. 10*, R84−R87.
13. Capili, A. D., Edghill, E. L., Wu, K., and Borden, K. L. B. (2004) Structure of the C-terminal RING finger from a RING-IBR-RING/TRIAD motif reveals a novel zinc-binding domain distinct from a RING. *J. Mol. Biol. 340*, 1117–1129.
14. (a) Borden, K. L. B. (1998) RING fingers and B-boxes: Zinc-binding protein-protein interaction domains. *Biochem. Cell Biol. 76*, 351–358. (b) Borden, K. L. B. (2000) RING domains: Master builders of molecular scaffolds. *J. Mol. Biol. 295*, 1103–1112.
15. Eisenhaber, B., Chumak, N., Eisenhaber, F., and Hauser, M.-T. (2007) The ring between RING fingers (RBR) protein family. *Genome Biol. 8*, 209–215.
16. Chang, F., Li, G., Haws, M., and Niu, T. (2007) Element concentrations in shell of *Pinctada magaritifera* from French Polynesia and evaluation for using as a food supplement. *Food Chem. 104*, 1171–1176.
17. Li, M., Liu, J., Ran, X., Fang, M., Shi, J., Qin, H., Goh, J. M., and Song, J. (2006) Resurrecting abandoned proteins with pure water: CD and NMR studies of protein fragments solubilized in salt-free water. *Biophys. J. 91*, 4201–4209.
18. Worthington, M. T., Amann, B. T., Nathans, D., and Berg, J. M. (1996) Metal binding properties and secondary structure of the zinc-binding domain of Nup475. *Proc. Natl. Acad. Sci. U.S.A. 93*, 13754–13759.
19. Michael, S. F., Kilfoil, V. J., Schmidt, M. H., Amann, B. T., and Berg, J. M. (1992) Metal binding and folding properties of a minimalist Cys_2His_2 zinc finger peptide. *Proc. Natl. Acad. Sci. U.S.A. 89*, 4796–4800.
20. Frankel, A. D., Berg, J. M., and Pabo, C. O. (1987) Metal-dependent folding of a single zinc finger from transcription factor I11A. *Proc. Natl. Acad. Sci. U.S.A. 84*, 4841–4845.
21. (a) Uversky, V. N. (2002) Natively unfolded proteins: A point where biology waits for physics. *Protein Sci. 11*, 739–756. (b) Tompa, P. (2002) Intrinsically unstructured proteins. *Trends Biochem. Sci. 27*, 527–533. (c) Uversky, V. N., Gillespie, J. R., and Fink, A. L. (2000) Why are "natively unfolded" proteins unstructured under physiologic conditions? *Proteins 41*, 415–427.
22. Greenfield, N. J. (2007) Using circular dichroism spectra to estimate protein secondary structure. *Nat. Protoc. 1*, 2876–2890.
23. Delak, K., Collino, S., and Evans, J. S. (2007) Expected and unexpected effects of amino acid substitutions on polypeptide-directed crystal growth. *Langmuir 23*, 11951–11955.
24. (a) Collino, S., Kim, I. W., and Evans, J. S. (2006) Identification of an "acidic" C-terminal mineral modification sequence from the mollusk shell protein, Asprich. *Cryst. Growth Des. 6*, 839–842. (b) Delak, K., Giocondi, J., Orme, C., and Evans, J. S. (2008) Modulation of crystal growth by the terminal sequences of the prismatic associated Asprich protein. *Cryst. Growth Des. 8*, 4481–4486.
25. Wustman, B. A., Weaver, J. C., Morse, D. E., and Evans, J. S. (2003) Characterization of a Ca(II)-, mineral-interactive polyelectrolyte sequence from the adhesive elastomeric biomineralization protein Lustrin A. *Langmuir 19*, 9373–9381.
26. (a) Kim, I. W., Morse, D. E., and Evans, J. S. (2004) Molecular characterization of the 30-AA N-terminal mineral interaction domain of the biomineralization protein AP7. *Langmuir 20*, 11664–11673. (b) Collino, S., and Evans, J. S. (2007) Structural features that distinguish kinetically distinct biomineralization polypeptides. *Biomacromolecules 8*, 1686–1694. (c) Collino, S., and Evans, J. S. (2008) The molecular specifications of a mineral modulation sequence derived from the aragonite-promoting protein, n16. *Biomacromolecules 9*, 1909–1918.
27. Metzler, R. A., Delak, K., Evans, J. S., Zhou, D., Beniash, E., Wilt, F., Abrecht, M., Chiou, J.-W., Guo, J., Coppersmith, S. N., and Gilbert, P. U. P. A. (2008) Probing the organic-mineral inteface (OMI) at the molecular level in model biominerals. *Langmuir 24*, 2680–2687.
28. (a) Evans, J. S. (2008) "Tuning in" to mollusk shell nacre- and prismatic-associated protein terminal sequences. Implications for biomineralization and the construction of high performance inorganic-organic composites. *Chem. Rev. 108*, 4455–4462. (b) Evans, J. S. (2003) Apples and oranges: Comparing the structural aspects of biomineral- and ice-interaction proteins. *Curr. Opin. Colloid Interface Sci. 8*, 48–54.
29. (a) Ragona, L., Catalano, M., Zetta, L., Longhi, R., Fogolari, F., and Molinari, H. (2002) Peptide models of folding initiation sites of bovine β-lactoglobulin: Identification of nativelike hydrophobic interactions involving G and H strands. *Biochemistry 41*, 2786–2796. (b) Buck, M. (1998) Trifluoroethanol and

colleagues: Cosolvents come of age. Recent studies with peptides and proteins. *Q. Rev. Biophys. 31*, 297–355. (c) Luo, P., and Baldwin, R. L. (1997) Mechanism of helix induction by trifluoroethanol: A framework for extrapolating the helix-forming properties of peptides from trifluoroethanol/water mixtures back to water. *Biochemistry 36*, 8413–8421. (d) Hong, D. P., Hoshino, M., Kuboi, R., and Goto, Y. (1999) Clustering of fluorine-substituted alcohols as a factor responsible for their marked effects on proteins and peptides. *J. Am. Chem. Soc. 121*, 8427–8433.

30. Kulp, J. L., III, Minamisawa, T., Shiba, K., and Evans, J. S. (2007) Conformational properties of an artificial protein that regulates the nucleation of inorganic and organic crystals. *Langmuir 23*, 3857–3863.
31. (a) Berman, A., Addadi, L., Kvick, A., Leiserowitz, L., Nelson, M., and Weiner, S. (1988) Intercalation of sea urchin proteins in calcite: Study of a crystalline composite material. *Science 250*, 664–666. (b) Albeck, S., Aizenberg, J., Addadi, L., and Weiner, S. (1993) Interactions of various skeletal intracrystalline components with calcite crystals. *J. Am. Chem. Soc. 115*, 11691–11697.
32. (a) Falini, G., Albeck, S., Weiner, S., and Addadi, L. (1996) Control of aragonite or calcite polymorphism by mollusk shell macromolecules. *Science 271*, 67–69. (b) Belcher, A. M., Wu, X. H., Christensen, R. J., Hansma, P. K., Stucky, G. D., and Morse, D. E. (1996) Control of crystal phase switching and orientation by soluble mollusc-shell proteins. *Nature 381*, 56–58.
33. Kim, I. W., Darragh, M. R., Orme, C., and Evans, J. S. (2006) Molecular "tuning" of crystal growth by nacre-associated polypeptides. *Cryst. Growth Des. 6*, 5–10.
34. Delak, K., Harcup, C., Lakshminarayanan, R., Zhi, S., Fan, Y., Moradian-Oldak, J., and Evans, J. S. (2009) The tooth enamel amelogenin is an intrinsically disordered protein with an extended molecular configuration in the monomeric form. *Biochemistry 48*, (submitted for publication).
35. Kapłon, T. M., Rymarczyk, G., Nocula-Ługowska, M., Jakób, M., Kochman, M., Lisowski, M., Szewczuk, Z., and Ozyhar, A. (2008) Starmaker exhibits properties of an intrinsically disordered protein. *Biomacromolecules 9*, 2118–2125.

BI802148R